GEOLOGICA CARPATHICA, APRIL 2013, 64, 2, 103–116 doi: 10.2478/geoca-2013-0007

Kinematically unrelated C–S fabrics: an example of extensional shear band cleavage from the Veporic Unit (Western Carpathians)

ZITA BUKOVSKÁ[1]✉, PETR JEŘÁBEK[1], ONDREJ LEXA[1], JIŘÍ KONOPÁSEK[2], MARIAN JANÁK[3] and JAN KOŠLER[2]

[1]Institute of Petrology and Structural Geology, Faculty of Science, Charles University in Prague, Albertov 6, 128 43 Prague 2, Czech Republic; ✉zita.bukovska@natur.cuni.cz
[2]Department of Earth Science and Center for Geobiology, University of Bergen, Allégaten 41, N-5007 Bergen, Norway
[3]Geological Institute, Slovak Academy of Sciences, Dúbravská cesta 9, P.O. Box 106, 840 05 Bratislava 45, Slovak Republic

(Manuscript received June 7, 2012; accepted in revised form September 18, 2012)

Abstract: Discontinuous and kinematically unrelated C–S fabrics have been recognized along the contact between the Gemeric and Veporic Units in the Western Carpathians. The formation of S and C fabrics within orthogneiss, quartzite and chloritoid-kyanite schist of the Veporic Unit is associated with Cretaceous syn-burial orogen-parallel flow and subsequent exhumational unroofing. The formation of the two fabrics characterized by distinct quartz deformation microstructure and metamorphic assemblage is separated by an inter-tectonic growth of transversal chloritoid-, kyanite-, ± monazite-bearing assemblage. The monazite U-Th-Pb concordia age of 97 ± 4 Ma was obtained by the laser ablation ICP–MS dating method. The age of this inter-tectonic metamorphic stage together with existing $^{40}Ar/^{39}Ar$ ages on exhumation of the Veporic Unit indicate that despite the similar appearance to shear bands or C–S mylonites there is a time span of at least 10 Myr between the formation of homogeneous S fabrics and superposed discrete C fabrics in the studied rocks.

Key words: Central Western Carpathians, Veporic Unit, structural geology, monazite dating, quartz deformation microstructure, shear band cleavage, discontinuous C–S fabrics.

Introduction

Shear bands refer to sub-parallel small-scale shear zones transecting an earlier anisotropy at small to intermediate angles which typically develop within larger-scale shear zones. These structures are associated with bulk simple shear or extension parallel to the earlier anisotropy and had been presented as shear bands (White 1979; Gapais & White 1982), C or C' bands (Berthé et al. 1979; Ponce & Choukroune 1980; Lister & Snoke 1984), extensional crenulation cleavage (Platt 1979, 1984; Platt & Vissers 1980) or shear band cleavage due to its cleavage-like appearance (White et al. 1980; Passchier & Trouw 2005). The main distinction between compressional crenulation cleavage and extensional shear band cleavage is based on the angle between cleavage and earlier foliation exhibiting 45–90° for compressional and less than 45° for extensional cleavage (Passchier & Trouw 2005). Therefore the shear band cleavage needs to be revealed by the complete C–S structure defined by pervasive anisotropy S "Schistosité" and discretely spaced cleavage C "Cisaillement" (Berthé et al. 1979). The main controversy related to the field interpretation of C–S fabrics is their temporal and kinematic relationship, since within a shear zone the C fabrics form either as a result of increasing strain or due to the overprint of an earlier kinematically unrelated anisotropy (Lister & Snoke 1984; Agard et al. 2011).

The contact zone between two major basement-cover thrust sheets, the hanging-wall Gemeric and footwall Veporic Units, in the Central Western Carpathians is characterized by complicated structure of Early Cretaceous imbrications modified by Late Cretaceous extension (Plašienka 1980, 1984; Lupták et al. 2000, 2003; Jeřábek et al. 2012). The extension resulted in the development of major shear zone associated with unroofing and exhumation of the Veporic Unit due to gravitationally-driven up-flow of middle crust in the core complex mode (Plašienka et al. 1999; Janák et al. 2001) or large-scale polyharmonic folding (Jeřábek et al. 2008, 2012). The C–S fabrics recognized within this shear zone have been previously interpreted as continuous kinematically related exhumation fabrics (Hók et al. 1993; Plašienka 1993; Lupták et al. 2003).

In this study, we aim to decipher the kinematically related versus unrelated nature of the C–S fabrics developed within a major extensional shear zone at the boundary between the Gemeric and Veporic Units in the Western Carpathians. The C–S fabrics were studied in orthogneiss, quartzite and chloritoid-kyanite schist across the shear zone, which allowed us to perform detailed structural, microstructural, metamorphic and geochronological characterization of the two fabrics. Furthermore based on our new data, the regional context of the complicated structure of the eastern part of the Gemeric and Veporic contact zone is discussed.

Geological setting

The Veporic Unit together with the Gemeric Unit to the east–southeast and Tatric Unit to the north (Fig. 1a) represent segments of Variscan crust that had been incorporated

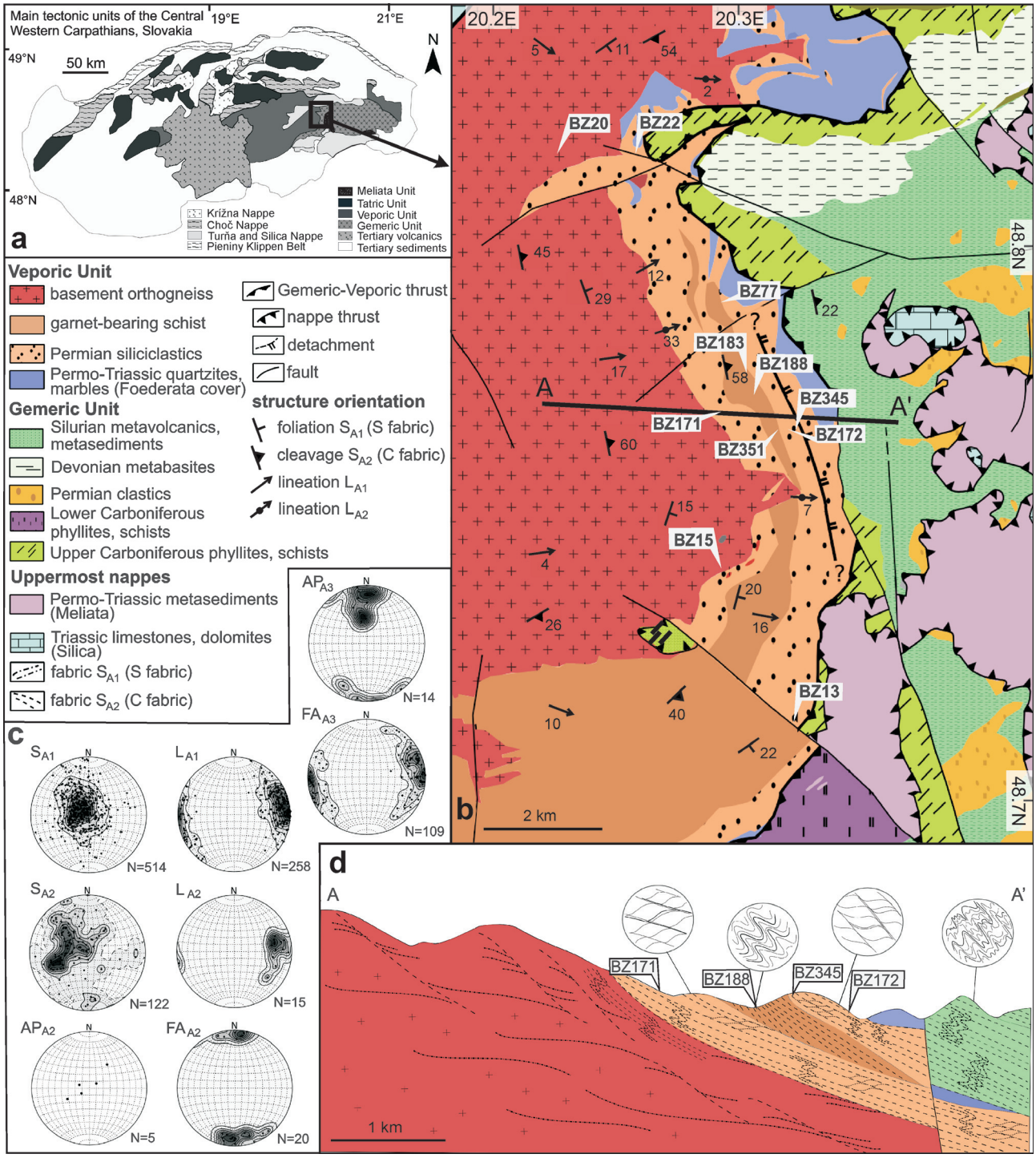

Fig. 1. a — Tectonic units of the Central Western Carpathians. **b** — Simplified geological and structural map of the studied area including location of the studied samples and structural cross-section A–A'; structural symbols show orientation of foliation S_{A1} (S fabric) and cleavage S_{A2} (C fabric), and accompanying lineations. Map based on Geological map of the Slovak Republic 1:50,000 http://mapserver.geology.sk. **c**— Lower hemisphere equal area projection of main structures documented in the studied area (S — foliation, L — lineation AP — fold axial plane, FA — fold axis, and A1–A3 — Alpine deformation events). Contours are double the multiples of standard deviation above the uniform distribution. **d** — Structural cross-section across the Gemeric-Veporic contact zone with macroscopic insets. GPS coordinates of selected localities: *BZ13* 48°42′15.38″N, 20°18′24.12″E; *BZ15* 48°43′55.91″N, 20°17′03.50″E; *BZ20* 48°48′10.32″N, 20°13′14.10″E; *BZ22* 48°48′20.97″N, 20°14′55.78″E; *BZ77* 48°46′46.52″N, 20°17′09.85″E; *BZ171* 48°47′45.69″N, 20°16′45.87″E; *BZ172* 48°45′20.16″N, 20°18′30.31″E; *BZ183* 48°45′48.61″N, 20°17′47.90″E; *BZ188* 48°45′34.55″N, 20°17′56.23″E; *BZ345* 48°45′17.49″N, 20°18′30.24″E; *BZ351* 48°45′18.65″N, 20°18′30.47″E.

into the structure of the Central West Carpathian wedge during the Cretaceous Eo-Alpine convergence (Plašienka et al. 1997). The Early Cretaceous thrust sheet stacking of the structurally lower Tatric, middle Veporic and upper Gemeric Unit (Tomek 1993; Plašienka et al. 1997) was followed by Late Cretaceous doming and exhumation of the deeper parts of the Veporic Unit (Janák et al. 2001; Jeřábek et al. 2012).

The studied area is located in the vicinity of the north-south trending contact between the footwall Veporic Unit and the hanging-wall Gemeric Unit (Fig. 1b). In this area, the Gemeric Unit comprises Lower Paleozoic volcano-sedimentary basement rocks of the Gelnica and Rakovec Groups marked by low- to medium-grade Variscan metamorphism (Faryad 1991) and overlying Upper Carboniferous–Permian metasedimentary cover (Vozárová & Vozár 1988). The Gemeric Unit is overthrust by the Meliata accretionary wedge complex of Jurassic age (Kozur & Mock 1973; Faryad & Henjes-Kunst 1997) and the uppermost Silica carbonate nappe system (Fig. 1a). Mostly low-grade Alpine metamorphic conditions have been determined for the Gemeric Unit (e.g. Petrasová et al. 2007). In the studied area, the Veporic Unit is characterized by an imbricated structure (Plašienka 1980, 1984) comprising from west to east and bottom to top (Fig. 1b,c): 1 — Variscan basement migmatite, orthogneiss and Carboniferous granitoids (Bibikova et al. 1988; Michalko et al. 1998); 2 — Permian cover quartzite; 3 — garnet-bearing schist; 4 — Permian cover quartzite-arcose marked by the presence of chloritoid-kyanite schist (Vrána 1964; Lupták et al. 2000) and 5 — Permo-Triassic quartzite and marble of the Foederata cover (Rozlosznik 1935; Schönenberg 1946). The garnet-bearing schists were traditionally related to the Veporic basement (Klinec 1966; Vrána 1966), however, on the basis of pollen analysis they have been later reinterpreted as Carboniferous metasediments of the Veporic cover belonging to the Slatviná Formation (Planderová & Vozárová 1978; Vozárová & Vozár 1988). The degree of Alpine metamorphic overprint reached amphibolite facies in the Veporic basement (up to 600 °C and 11 kbar; Vrána 1966; Janák et al. 2001; Jeřábek et al. 2008) and greenschist facies in the Foederata cover (up to 380 °C and 4.5 kbar; Lupták et al. 2003). The metamorphic conditions of chloritoid-kyanite schists have been estimated as 530–560 °C and 6–8 kbar (Lupták et al. 2000). The southern part of the studied area has been later affected by HT-LP contact metamorphism related to the intrusion of Upper Cretaceous Rochovce I-type granite (Kamenický 1977; Klinec et al. 1980; Vozárová 1990; Hraško et al. 1998; Poller et al. 2001).

Structural record in the studied area

Within the hanging-wall Gemeric Unit, we identified one penetrative metamorphic foliation overprinted by two phases of folding. The greenschist facies metamorphic foliation S_V recognized exclusively in the Lower Paleozoic rocks of the Gemeric Unit is regarded as it was by other authors (e.g. Hovorka et al. 1988; Faryad 1990) as the result of a Variscan tectono-metamorphic event. This foliation shows various orientations due to subsequent folding characterized by steep or south facing and generally E-W trending axial planes or low-grade spaced cleavage. On the scale of the Gemeric Unit, this latter cleavage forms large-scale positive fan-like structure interpreted as a result of the Early Cretaceous overthrusting of the Gemeric Unit over the Veporic (Snopko 1971; Lexa et al. 2003). In the proximity of the Gemer-Vepor boundary, both Variscan fabrics and steep Early Alpine cleavage are affected by isoclinal folding with subhorizontal axial planes and E-W trending axes.

In the footwall Veporic Unit, we recognized three deformation-metamorphic fabrics which were subsequently affected by one folding event. The oldest deformation fabric comprises scarce relics of high-grade Variscan foliation S_V in basement migmatites and schists. The first Alpine metamorphic foliation S_{A1} heterogeneously affects both basement and cover and dips generally to the E or SE under shallow to intermediate angles (Fig. 1b,c). The S_{A1} fabric bears mineral and stretching lineation L_{A1} defined by shape preferred orientation of quartz aggregates and white mica, which plunges generally to the east (Fig. 1b,c). The S_{A1} is axial planar to the locally preserved isoclinal folds affecting Variscan foliations in the basement and bedding in the cover. The fold axes are typically E-W trending and so subparallel to lineation L_{A1}. In the basement, the S_{A1} is only heterogeneously overprinted by discrete S_{A2} cleavage, while in the cover the S_{A2} becomes dominant deformation fabric. This late cleavage dips to the E or SE at steeper angles than the foliation S_{A1} and bears an east-plunging mostly muscovite-bearing lineation (Fig. 1c). The S_{A2} is axial planar to the locally developed isoclinal folds F_{A2} characterized by N-S trending axes. The S_{A2} is defined mainly by shape preferred orientation of chlorite and white mica. The last deformation event is associated with upright folding of all previous fabrics and led to the development of small-scale crenulations as well as large-scale folds F_{A3} with generally E-W trending axial planes (Fig. 1b,c). This late stage folding is associated with the development of a sinistral transpressional shear zone along the NE-SW trending Gemer-Vepor boundary to the south from the studied area (Lexa et al. 2003).

In the studied area, the S_{A1} and S_{A2} fabrics typically show the low angle extensional shear band cleavage relationships characterized by discrete cleavage S_{A2} cross-cutting the foliation S_{A1} (Fig. 2) and thus in the subsequent text, the two fabrics will be referred to as C and S fabrics, respectively. These C–S fabrics form an angle ranging between 10 and 30° and are characterized by the normal top-to-the-east sense of shear. The L_{A1} and L_{A2} lineations (Fig. 1c) are both perpendicular to the C–S intersection implying the synkinematic character of the two fabrics (Passchier & Trouw 2005).

Analytical techniques

The C–S fabrics in the Veporic Unit were analysed in orthogneiss, chloritoid-kyanite schist and quartzite (Figs. 2 and 3a), which allowed us to characterize both fabrics in terms of quartz deformation microstructure and texture, metamorphism and age. The analyses were performed on the thin sections parallel to the XZ plane of finite strain ellipsoid,

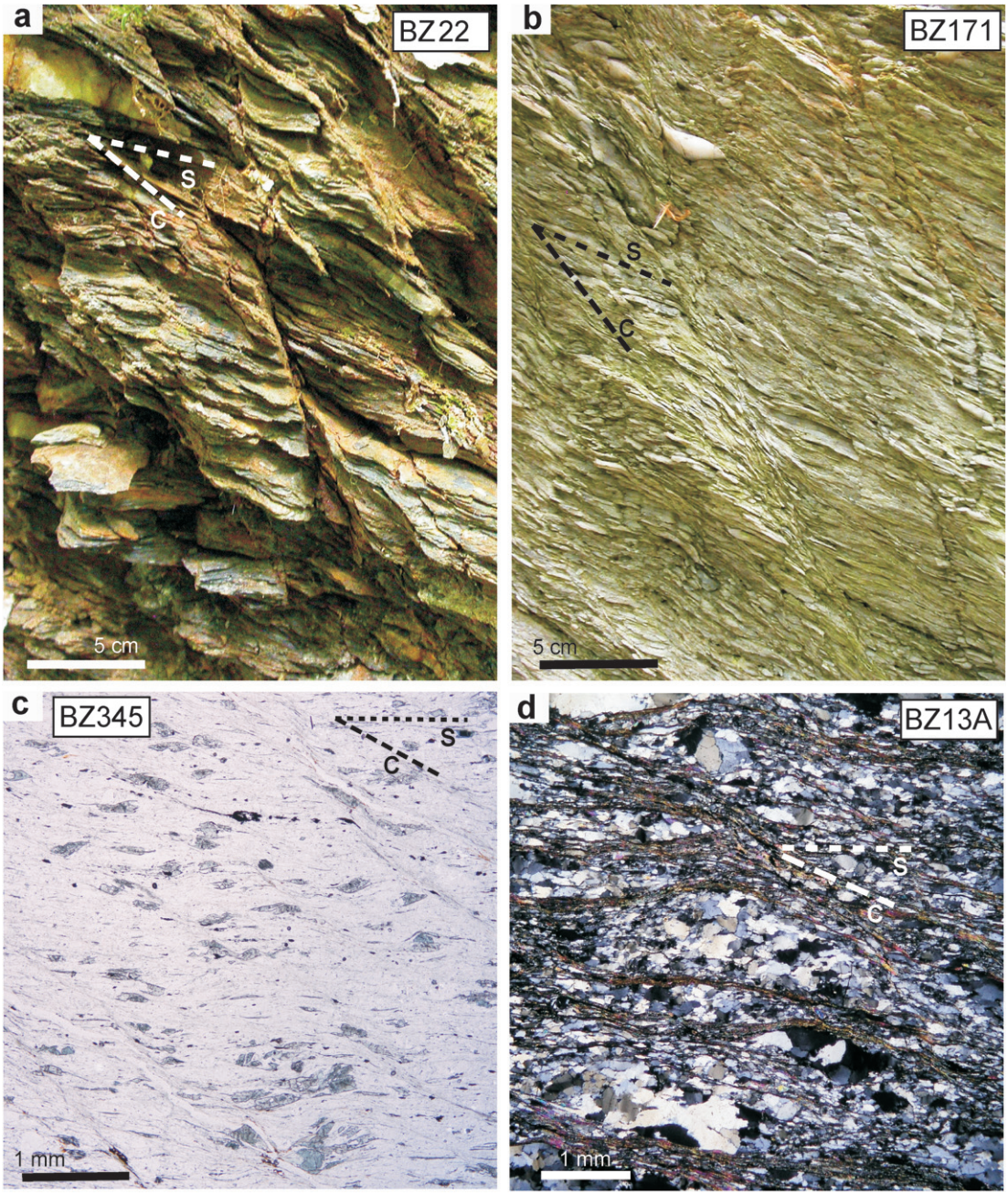

Fig. 2. Field photographs (a, b) and micrographs (c, d) of C–S fabrics in the Veporic Unit: **a** — basement schist, **b** — Permian quartzite, **c** — chloritoid-kyanite schist, **d** — quartzite (crossed polarizers).

namely parallel to L_{A1} and L_{A2} lineations and perpendicular to intersection of C–S fabrics.

Quartz deformation microstructure have been quantitatively analysed by means of the Computer Integrated Polarization microscopy (CIP) technique of Panozzo Heilbronner & Pauli (1993) and the Electron Backscatter Diffraction (EBSD) technique using the HKL system attached to the scanning electron microscope TESCAN at the Institute of Petrology and Structural Geology, Charles University in Prague. The grain size and grain shape statistics were obtained from manually digitized grain maps based on CIP-derived misorientation images (Heilbronner 2000) using the PolyLX Matlab toolbox (Lexa 2003). In this paper, the average 2D grain size is defined as 1 sigma range of the area weighted logarithmic mean of equal area diameter. The grain shapes are characterized by particle (PAROR) and surface (SURFOR) orientation distribution functions (ODF) (Panozzo 1983, 1984) shown in the rose diagrams.

Chemical analyses of selected minerals were carried out using a EDS detector X-Max 50 (Oxford Instruments) attached to the scanning electron microscope TESCAN Vega at the Institute of Petrology and Structural Geology, Charles University in Prague. The analyses were obtained with accelerating potential 15 kV and beam current 1 nA. Matrix cor-

rection procedure XPP was used based on Phi-Rh-Z method. The precision control was held by repeated analysis measurements on known phases, mainly standards. Standards that were used for each analysed element (element, detection limit of 2 sigma in weight %): albite (Na, 0.1); synthetic periclase (Mg, 0.04); synthetic $Y_3Al_5O_{12}$ (Al, 0.1); sanidine (Si, 0.16); sanidine (K, 0.04); wollastonite (Ca, 0.04); synthetic rutile (Ti, 0.06); synthetic Cr_20_3 (Cr, 0.06); rhodonite (Mn, 0.08); hematite (Fe, 0.08); pentlandite (Mn, 0.12).

Chloritoid analyses were normalized to 12 oxygens, chlorite was normalized to 14 oxygens and white mica analyses were normalized to 11 oxygens (see Table 1). The classification of white mica followed Tischendorf et al. (2004). X_{Mg} is defined as $X_{Mg} = Mg/(Mg+Fe)$.

U-Th-Pb dating of monazite was performed directly from polished thin sections by laser ablation ICP–MS analysis following the technique described in Košler et al. (2001). A Thermo-Finnigan Element 2 sector field ICP–MS coupled to a 193 nm ArF excimer laser (Resonetics RESOlution M-50 LR) at Bergen University was used to measure Pb/U and Pb/Th isotopic ratios. The laser was fired at 5 Hz using energy of 40 mJ/pulse and beam diameter of 7 micrometers, while the sample was moved underneath the laser beam to produce linear raster pits (<5 μm deep) in the monazite grains. The ablation was done in He (0.65 l/min). A fragment of a large monazite crystal from a granulite in the Androyan Complex in Madagascar (555 Ma: U-Pb TIMS age by R. Parrish, pers. comm. and 557±20 Ma: electron microprobe chemical dating by Montel et al. 1996) was used to calibrate the Tl-Bi-Np tracer solution that was analysed simultaneously with the ablated monazite samples. In addition, two monazite samples with known TIMS ages (Tarasinga leptynite, India, 953±4 Ma — Aftalion et al. 1988; and garnetiferous gneiss from the Lake Baikal Complex, Russia, 1862±4 Ma — Aftalion et al. 1991) were periodically analysed during this study for quality control and yielded concordia ages of 957±43 Ma (n=5) and 1868±89 Ma (n=3), respectively (n=number of analyses; all uncertainties are 2 sigma).

Quartz deformation microstructure

All studied samples show two distinct quartz microstructures related to S and C fabrics as exemplified by two samples in Fig. 3a, namely orthogneiss sample BZ15 and quartzite sample BZ77 (for location see Fig. 1). The S fabrics are defined by recrystallized quartz aggregates with larger grain size, which are cross-cut or modified by localized C fabrics forming tails of recrystallized grains with considerably smaller grain size (Fig. 3a). The aggregates show grain size within the ±1 sigma range of 45–184 μm (d_{mean}=91 μm) for orthogneiss and 140–403 μm (d_{mean}=237 μm) for quartzite, while the tails show grain size within the range of 20–56 μm (d_{mean}=33 μm) for orthogneiss and 47–140 μm (d_{mean}=81 μm) for quartzite (Fig. 3d).

The quartz grains are strongly elliptical in orthogneiss aggregates while the grains in tails from both lithologies and quartzite aggregates show weak ellipticity (Fig. 3a). The shape preferred orientation of quartz grains characterized by particle ODF (PAROR) is subparallel to the long axis of either the

Table 1: Representative chemical analyses of muscovite (Ms), phengite (Ph) and chlorite (Chl) from orthogneiss sample BZ20B, chloritoid (Cld), chlorite (Chl), margarite (Mrg), paragonite (Pg) and muscovite (Ms) from chloritoid-kyanite schist samples BZ183, BZ349 and BZ351H and garnet core and rim (GtI, GtII) from garnet-bearing schist BZ188 (for location of samples see Fig. 1).

mineral	Ms I	Ph	Ms II	Chl	Pg	Mrg	Cld	Ms	Chl	Gtl	Gtll	Amp
sample		BZ20B			BZ349	BZ351H	BZ351H	BZ183	BZ349		BZ188	
lithology		orthogneiss				chloritoid-kyanite schist					amphibole-garnet schist	
SiO_2	45.85	50.80	47.72	35.99	45.09	37.01	23.09	46.06	23.89	36.29	36.91	41.96
TiO_2	0.67	0.37	0.41	1.62	0.00	0.00	0.00	0.21	0.00	0.03	0.12	0.42
Cr_2O_3	0.00	0.00	0.00	0.00	0.00	0.00	0.00	0.00	0.00	0.00	0.00	0.00
Al_2O_3	32.68	29.63	34.21	17.12	40.55	46.80	38.97	36.29	21.74	20.76	21.00	15.87
FeO	2.43	1.85	1.91	16.12	0.73	1.01	22.71	2.18	24.36	31.98	29.97	17.32
MnO	0.00	0.00	0.00	0.18	0.00	0.00	0.41	0.00	0.00	5.73	3.06	0.00
NiO	0.00	0.00	0.00	0.00	0.00	0.00	0.00	0.00	0.00	0.00	0.00	0.00
MgO	1.91	2.59	1.53	11.57	0.00	0.08	4.00	0.55	14.42	2.64	1.70	8.13
CaO	0.00	0.00	0.00	0.00	0.55	6.57	0.00	0.00	0.00	2.03	7.68	10.37
Na_2O	0.27	0.11	0.23	0.00	6.77	3.26	0.00	1.13	0.00	0.00	0.00	1.60
K_2O	10.72	10.68	10.56	9.81	0.99	1.01	0.00	9.13	0.00	0.00	0.00	0.40
Total	**94.52**	**96.02**	**96.57**	**92.42**	**94.67**	**95.75**	**89.17**	**95.54**	**84.42**	**100.45**	**99.46**	**96.06**
Si	3.09	3.38	3.15	3.48	2.91	2.40	1.96	3.06	2.61	2.95	2.95	6.23
Ti	0.03	0.02	0.02	0.12	0.00	0.00	0.00	0.01	0.00	0.00	0.01	0.05
Cr	0.00	0.00	0.00	0.00	0.00	0.00	0.00	0.00	0.00	0.00	0.00	0.00
Al	2.59	2.32	2.66	1.95	3.08	3.58	3.90	2.84	2.80	1.99	1.98	2.77
Fe^{3+}	0.12	0.00	0.00	0.00	0.02	0.05	0.19	0.00	0.00	0.11	0.11	2.15
Fe^{2+}	0.02	0.10	0.11	1.30	0.02	0.00	1.42	0.12	2.23	2.06	1.89	0.00
Mn	0.00	0.00	0.00	0.01	0.00	0.00	0.03	0.00	0.00	0.39	0.21	0.00
Ni	0.00	0.00	0.00	0.00	0.00	0.00	0.00	0.00	0.00	0.00	0.00	1.80
Mg	0.19	0.26	0.15	1.67	0.00	0.01	0.51	0.05	2.35	0.32	0.20	1.65
Ca	0.00	0.00	0.00	0.00	0.04	0.46	0.00	0.00	0.00	0.18	0.66	0.46
Na	0.04	0.01	0.03	0.00	0.85	0.41	0.00	0.15	0.00	0.00	0.00	0.08
K	0.92	0.91	0.89	1.21	0.08	0.08	0.00	0.77	0.00	0.00	0.00	0.00
Total	**7**	**7**	**7**	**10**	**7**	**7**	**8**	**7**	**10**	**8**	**8**	**15.18**
X_{Mg}	0.58	0.59	0.71	0.56	0.00	0.13	0.24	0.31	0.51	0.13	0.10	0.58

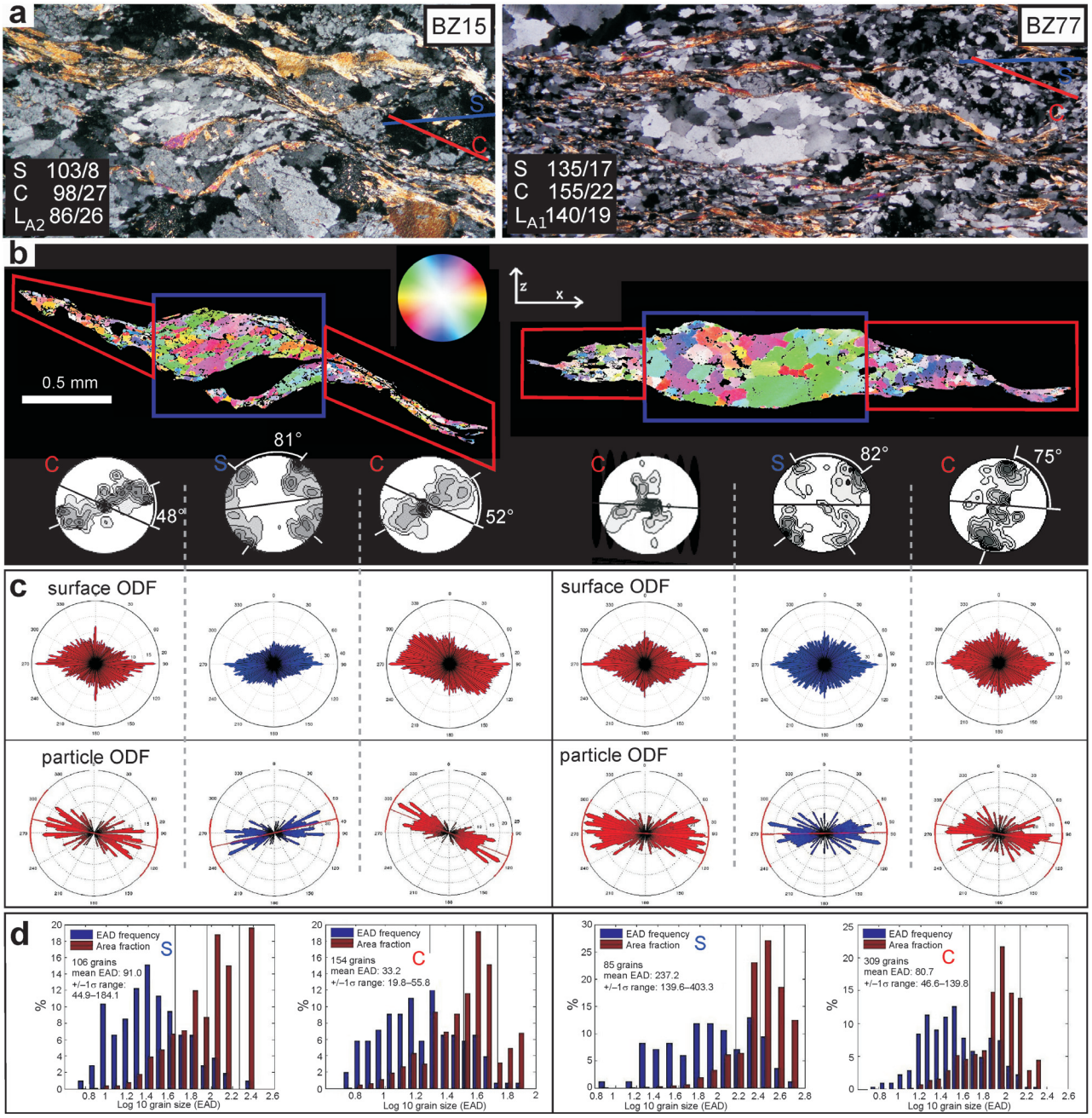

Fig. 3. Quartz microstructure within S and C fabrics from orthogneiss sample BZ15 (left column) and quartzite sample BZ77 (right column). **a** — Micrograph (crossed polarizers) of C–S fabrics shows recrystallized quartz aggregates within S fabric and tails within C fabric. **b** — quartz c-axis CPO images and corresponding lower hemisphere equal area pole figures from S aggregates and C tails. The c-axis orientation colouring of individual grains is shown in colour look-up table pole figure. The black lines in the pole figures correspond to the long axis of S aggregates and C tails, and the contours correspond to multiples of uniform distribution. **c** — Surface (SURFOR) and particle (PAROR) orientation distribution functions for S aggregates and C tails. **d** — Quartz grain size distributions within S aggregates and C tails manifested by 2D equal area diameter (EAD) frequency and area fraction (in μm). The average 2D grain size defined as 1 σ range of area weighted logarithmic mean of EAD and number of grains are also shown in the histograms.

S fabric aggregates or C fabric tails (Fig. 3c). The surface ODF (SURFOR) in quartzite aggregates shows symmetrical distribution with maximum parallel to the aggregate long axis. In quartzite tails, the surface ODF is weakly monocline with a maximum that is slightly inclined with respect to the tail orientation. In orthogneiss, the surface ODF is weakly to strongly monocline with maxima that are slightly and strongly inclined with respect to aggregate and tail orientation, respectively (Fig. 3c). Within the C fabrics, the inclination of surface ODF maxima with respect to C tails orientation is consistent with the observed macroscopic sense of shear (e.g. Simpson & Schmid 1983).

Quartz texture

The crystal preferred orientation (CPO) of quartz c-axes shows similar patterns for both orthogneiss and quartzite samples. Within the aggregates defining the S fabric, the c-axis CPOs are characterized by two-point peripheral maxima, which are symmetrically distributed around the aggregate long axis at the distance of approximately 50° (Figs. 3b, 4a). Additionally, the aggregate in orthogneiss sample BZ15 shows two-point peripheral c-axis submaxima distributed symmetrically around the aggregate long axis within ~15° distance. On the other hand, the aggregate in quartzite sample BZ77 shows minor c-axis submaximum in the centre of the pole figure. The aggregate double point maxima in both samples are interpreted as results of activity of the basal ⟨a⟩ slip system while the submaxima suggest prism ⟨a⟩ slip in the case of quartzite and prism [c] slip in the case of orthogneiss (e.g. Schmid & Casey 1986). By using the fabric opening thermometer of Kruhl (1996, 1998) modified by Morgan & Law (2004), the c-axis opening angle of ~80° (Figs. 3b, 4a) corresponds to ~550 °C.

Within the tails defining the C fabric, the c-axis CPOs show single girdle patterns inclined with respect to C planes (Figs. 3b, 4b,c). This inclination is more pronounced in orthogneiss sample BZ15 compared to quartzite sample BZ77 as indicated by the angle of 46–52° and 75° between the single girdle trace and C fabric trace in the pole figures (Figs. 3b, 4b,c). The highly inclined c-axis single girdle pattern is characteristic for combined activity of rhomb ⟨a⟩ and prism ⟨a⟩ slip systems (Keller & Stipp 2011) and suggests a normal sense of shearing along the C planes (Lister & Williams 1979; Simpson & Schmid 1983; Schmid & Casey 1986).

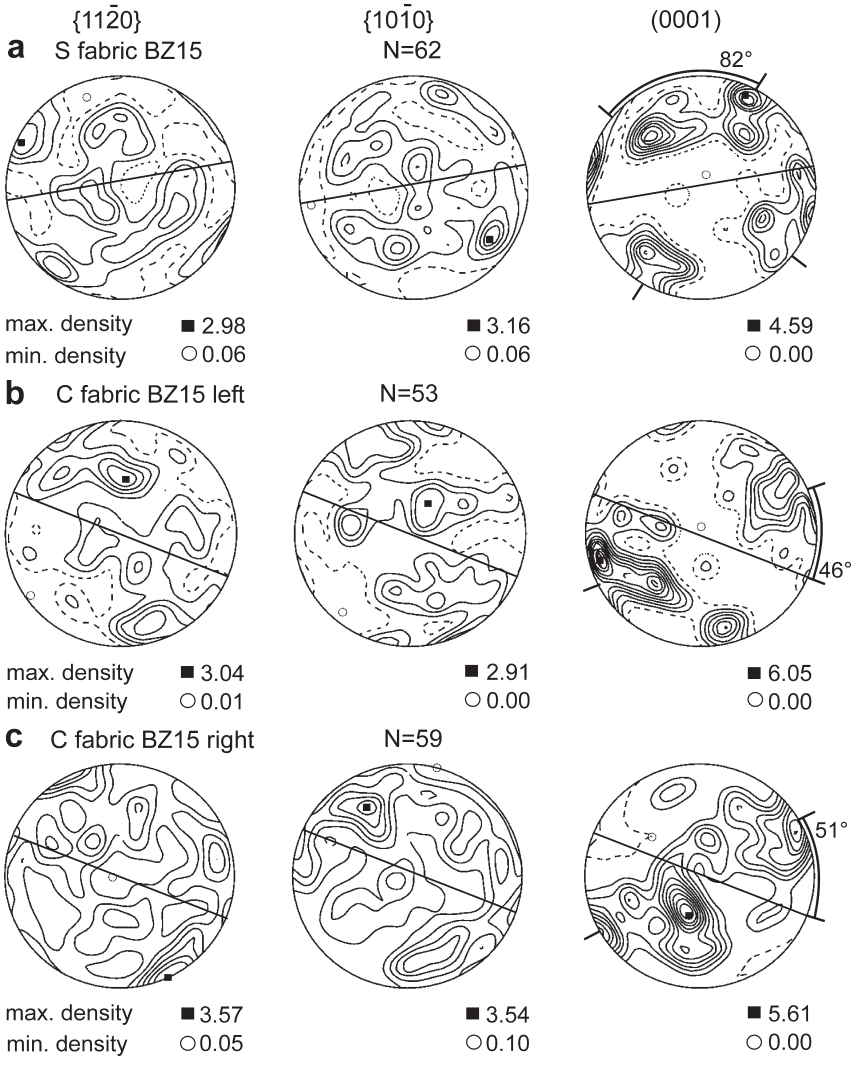

Fig. 4. The lattice preferred orientation data of recrystallized quartz within S aggregate (**a**) and C tail (**b**, **c**) in sample BZ15 (same region as in Fig. 3, **a** — center, **b** — left, **c** — right) obtained by means of electron back-scattered diffraction (EBSD). Each pole figure in lower hemisphere equal area projection contains the number of measured grains, minimum and maximum of the density distribution and contours corresponding to 0.5 multiples of uniform distribution.

Petrography and mineral chemistry

Within the imbricated structure of the studied area several lithologies have been evaluated by means of petrography and mineral chemistry. These are from bottom to top: 1 — basement orthogneiss; 2 — cover quartzite (lower package, see Fig. 1c); 3 — basement garnet-bearing schist; 4 — chloritoid-kyanite schist of probably cover affinity and 5 — cover quartzite (upper package, Fig. 1b,c). The studied cover rocks are distinguished as the Rimava Formation (Plašienka et al. 1997). In orthogneiss and chloritoid-kyanite schist, the analysis revealed that both S and C fabrics are associated with distinct metamorphic records.

In orthogneiss, the S fabric is defined by metamorphic mineral assemblage of biotite, chlorite, white mica, albite and quartz. In contrast, the discrete C fabric contains only chlorite, white mica and quartz. While chlorite in both fabrics shows identical composition to (X_{Mg}=0.56, sample BZ20B, Table 1), the chemical analyses of white mica revealed three generations that include muscovite I, phengite and muscovite II (sample BZ20B in Figs. 5a,b and 6a). The first generation of white mica (muscovite I) is represented by large flakes (ca. 1 mm in size) that are associated neither with the S, nor the C fabric and are probably of magmatic origin (Fig. 4a). The Si content in muscovite I varies between 3.09–3.15 a.p.f.u. (Table 1, Fig. 6a). Muscovite I flakes are overgrown by a second generation of white mica (phengite) which is com-

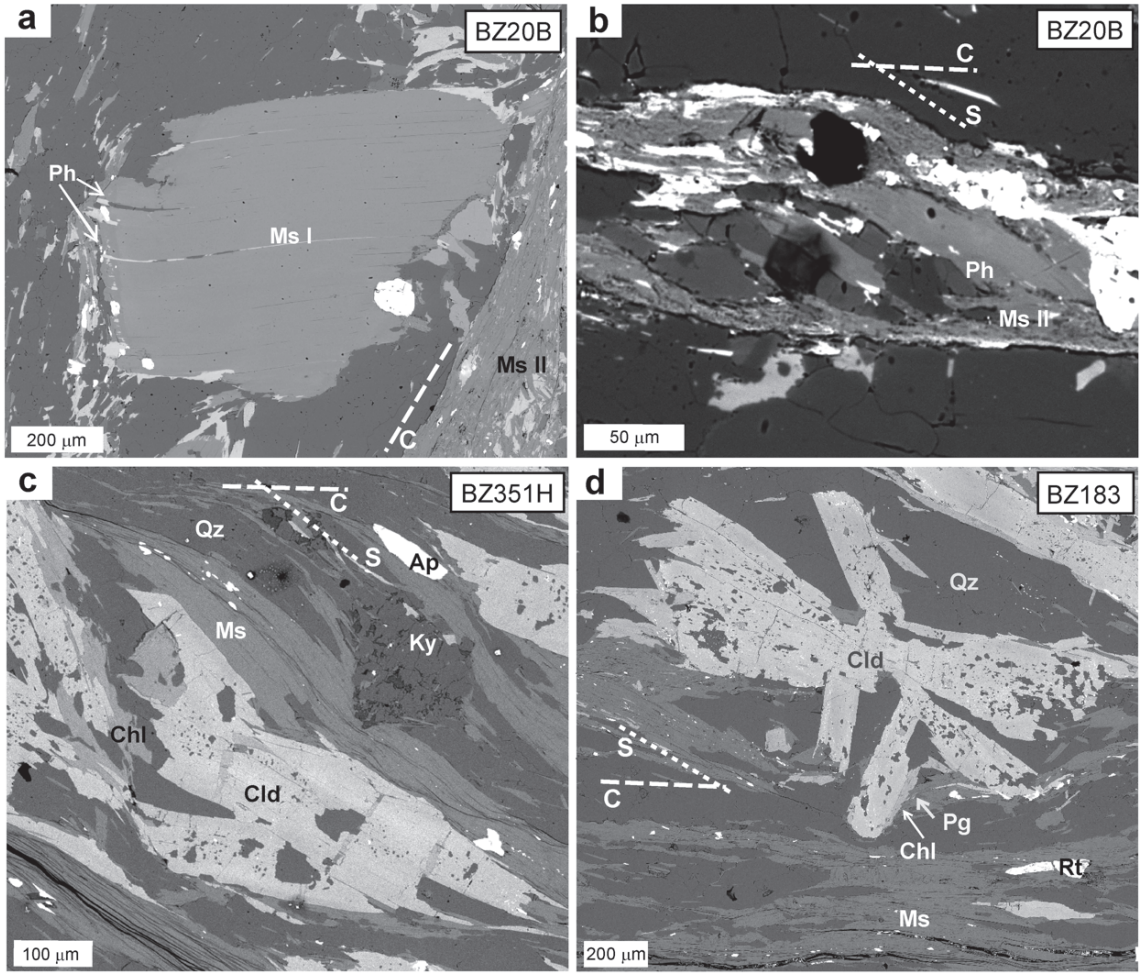

Fig. 5. BSE images showing white micas in orthogneiss sample BZ20B (**a**, **b**) and mineral assemblage in chloritoid schist samples BZ351H (**c**) and BZ183 (**d**) and their relation to C–S fabrics. **a** — Large muscovite grain (Ms I) overgrown by phengite (Ph) and younger muscovite (Ms II) within C fabric. **b** — Phengite within S fabric replaced by muscovite II within C fabric. **c, d** — Peak assemblage of kyanite, chloritoid, white mica, chlorite and quartz in chloritoid-kyanite schist associated with S fabric being cross-cut by C fabric defined by muscovite-chlorite. **Mineral abbreviations:** Ap — apatite, Chl — chlorite, Cld — chloritoid, Ky — kyanite, Ms — muscovite, Pg — paragonite, Ph — phengite, Qz — quartz, Rt — rutile.

mon in the S fabric (Fig. 5a,b). In accordance with the classification of Tischendorf et al. (2004), this white mica is phengite and contains 3.27–3.38 a.p.f.u. of Si (Table 1, Fig. 6a). The last generation of white mica (muscovite II) with 3.1–3.15 a.p.f.u. of Si (Table 1, Fig. 6a) replaces the earlier phengite and it is associated with the C fabrics (Fig. 5a,b). An identical compositional sequence of white mica was previously reported from the Veporic basement by Sulák et al. (2009), however, in their study no relationship to the deformation structures has been revealed.

The overlying lower cover package quartzite (sample BZ171) consists of quartz, phengite, monazite, zircon and ilmenite. The chemical analysis of white mica did not reveal major compositional differences between S and C fabrics in individual samples. The white mica in quartzite samples located closer to the basement orthogneiss is phengite with 3.11–3.34 a.p.f.u. of Si (Fig. 6b).

The overlying garnet-bearing schist typically consists of quartz, biotite, muscovite, chlorite, ilmenite, ± garnet and ± tschermakite. In sample BZ188 located near the chloritoid-kyanite schists (Fig. 1b), the garnet consists of two compositional varieties (Fig. 7) with core garnet (GtI) rich in magnesium, manganese and iron (alm_{60-70}, sps_{9-13}, prp_{9-12}, grs_{5-6}, Fig. 7, Table 1) and rim garnet (GtII) enriched in calcium (alm_{57-62}, grs_{20-22}, prp_{6-7}, sps_{5-6}, Fig. 7, Table 1). Such a compositional zoning has been previously described from identical garnet-bearing schist from the Blh Valley by Korikovsky et al. (1990) and Jeřábek et al. (2008). On the basis of PT calculations the later authors relate the garnet core and rim to the Variscan and Alpine metamorphism, respectively, implying the basement origin of these schists (Vrána 1964; Korikovsky et al. 1990; Jeřábek et al. 2008).

The Rimava Formation chloritoid-kyanite schist located at the contact between the basement schist and Permian cover quartzite (samples BZ351H, BZ345 and BZ183) consists of kyanite, chloritoid, white mica, chlorite, quartz ± tourmaline and accessory apatite, ilmenite, rutile, zircon ± monazite ± allanite ± xenotime (Fig. 5c,d). The chloritoids show radial-

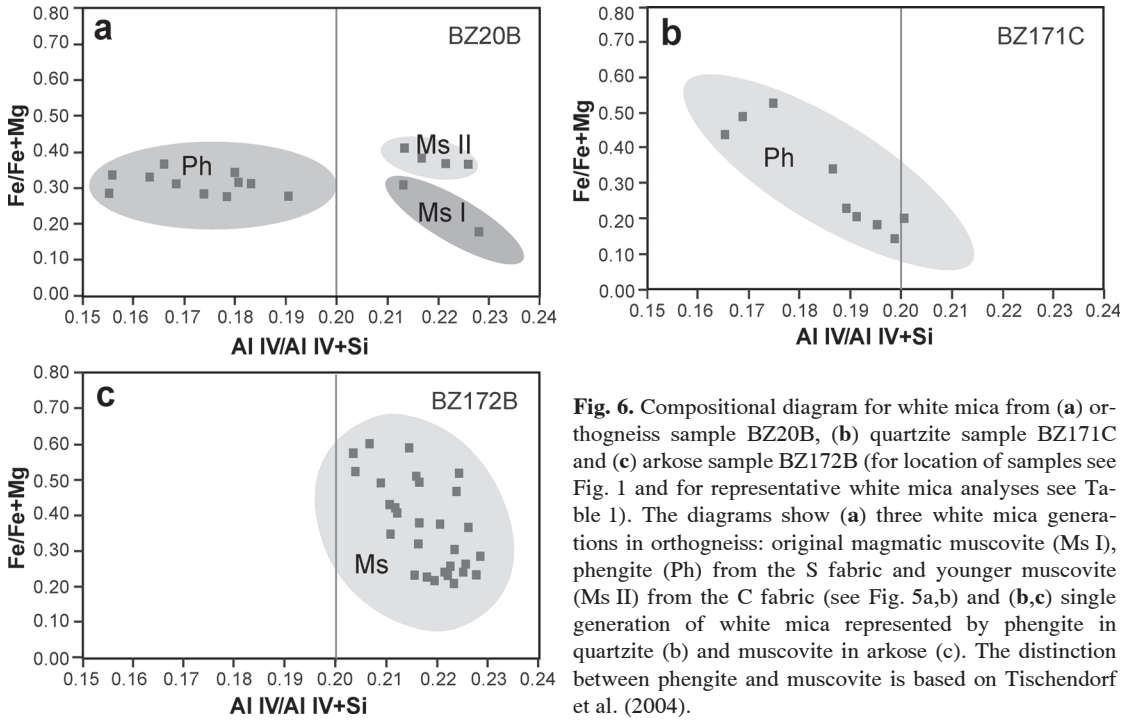

Fig. 6. Compositional diagram for white micas from (**a**) orthogneiss sample BZ20B, (**b**) quartzite sample BZ171C and (**c**) arkose sample BZ172B (for location of samples see Fig. 1 and for representative white mica analyses see Table 1). The diagrams show (**a**) three white mica generations in orthogneiss: original magmatic muscovite (Ms I), phengite (Ph) from the S fabric and younger muscovite (Ms II) from the C fabric (see Fig. 5a,b) and (**b**,**c**) single generation of white mica represented by phengite in quartzite (b) and muscovite in arkose (c). The distinction between phengite and muscovite is based on Tischendorf et al. (2004).

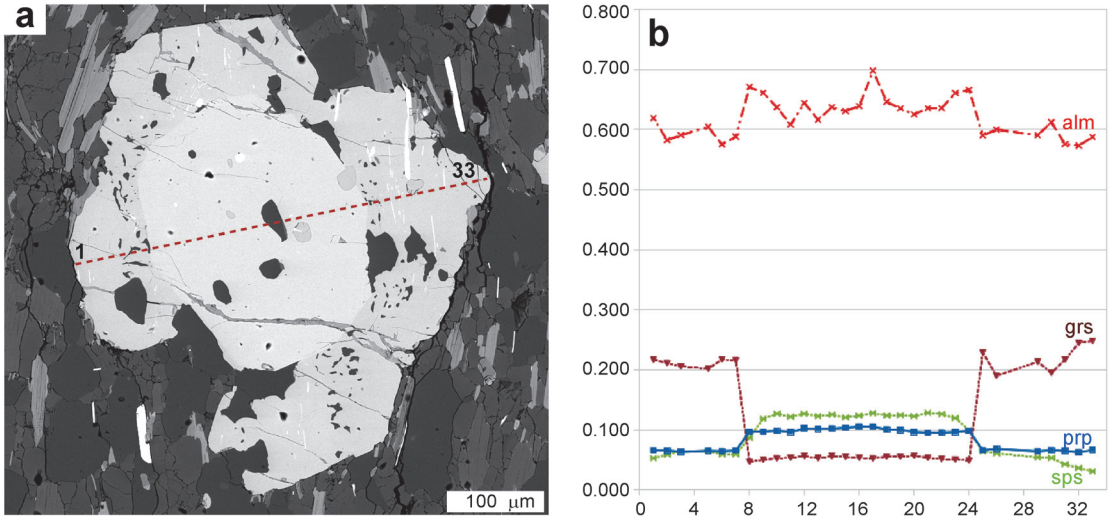

Fig. 7. a — BSE image showing garnet from tschermakite-garnet schist with orientation of compositional profile (sample BZ188). **b** — Compositional profile across garnet grain.

growth appearance which is commonly transversal to the S fabric and cross-cut by the C fabric (Figs. 2c, 5c,d). This indicates an inter-tectonic growth of the kyanite, chloritoid, white mica, chlorite, monazite and quartz assemblage. The chemical analyses of white mica revealed the presence of muscovite, paragonite and margarite, associated with a chloritoid- and kyanite-bearing assemblage (Table 1, Fig. 6d). The X_{Mg} in chloritoid within different samples ranges between 0.17–0.34 and shows slight but irregular zoning. Within individual samples the X_{Mg} in chloritoid differs mostly by 0.02–0.09. The C fabrics are characterized by muscovite, chlorite and quartz assemblage. The chemical composition of chlorite and muscovite associated with S and C fabrics, respectively, did not reveal major differences so that the X_{Mg} in chlorite is ~0.51 and the Si content in muscovitic mica ranges between 2.95–3.08 a.p.f.u.

The upper cover package quartzites and arkoses are formed by white mica-quartz ± chlorite ± albite and accessory ilmenite, rutile ± apatite ± zircon ± monazite (Fig. 2d). The chemical analysis of white mica did not reveal major compositional differences between S and C fabrics in individual samples. The rock is phengite absent comparing to the cover quartzites (BZ171). White mica is muscovite with 3.09–3.19 a.p.f.u. of Si (BZ172B in Fig. 6c; for location see Fig. 1).

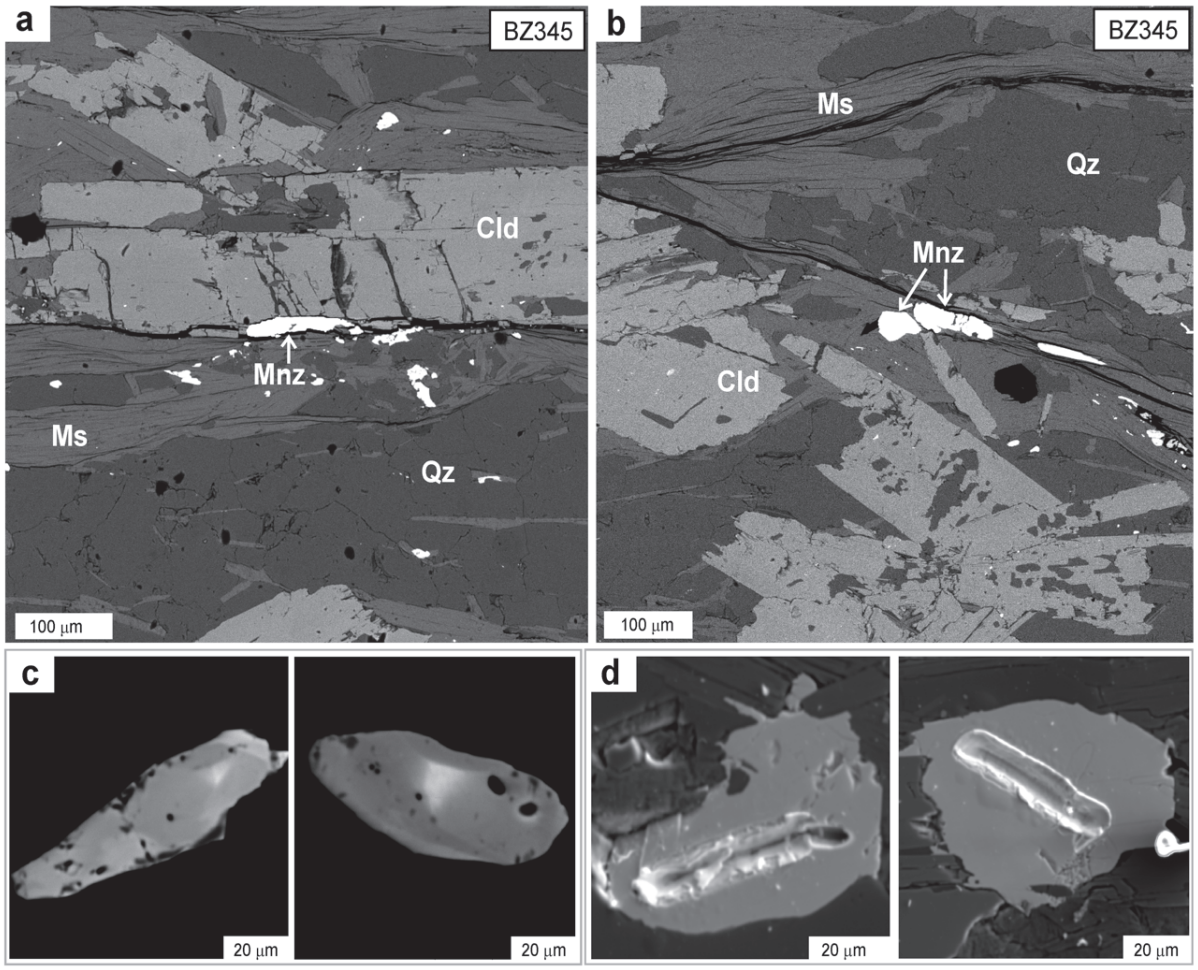

Fig. 8. a, b — BSE images showing close relationship of dated monazite (Mnz) and chloritoid in chloritoid-kyanite schist sample BZ345. **c** — Detailed BSE images show relatively homogeneous chemical composition of dated monazite grains. **d** — SE images show positions of analysed sections within monazite grains. For mineral abbreviations see Fig. 5 caption.

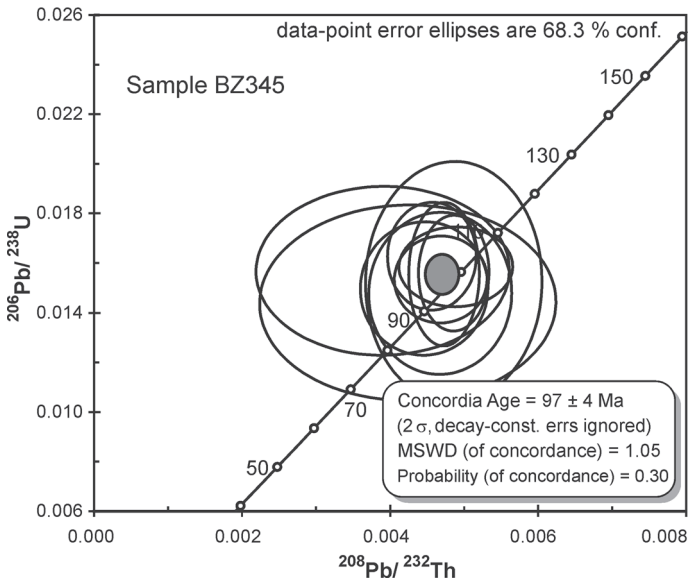

Fig. 9. U-Th-Pb concordia diagram for monazite from sample BZ345. For isotopic ratios see Table 2.

Monazite dating

Monazite was identified in the chloritoid- and kyanite-bearing schist (sample BZ345; for location see Fig. 1) as subhedral to anhedral, usually elongated grains of ~50–100 μm in length. Monazite occurs either within the recrystallized quartz aggregates or as grains completely enclosed by muscovite. Many monazite grains show sharp, non-altered contacts with chloritoid and other mineral phases of this kyanite, chloritoid, white mica, chlorite and quartz assemblage (Fig. 8a,b), which suggests that monazite is a stable member of this inter-tectonic (see above) assemblage. The high resolution back-scattered electron images of several monazite grains revealed some compositional variations (Fig. 8c), however the spatial resolution of laser ablation did not allow analysis of the small compositionally different domains. Monazite grains were analysed directly in polished thin sections (Fig. 8d). Ten selected monazite grains analysed in sample BZ345 (Table 2) yielded a pooled U-Th-Pb concordia age of 97±4 Ma (±2 sigma, Fig. 9, Table 2), which is interpreted as the monazite crystallization age.

Table 2: Laser ablation ICP-MS U-Th-Pb data for the sample BZ345. Only $^{208}Pb/^{232}Th$ and $^{206}Pb/^{238}U$ isotopic ratios and corresponding ages are presented. Determination of $^{207}Pb/^{206}Pb$ and $^{207}Pb/^{235}U$ ages was precluded by low signal intensity of ^{207}Pb.

Analysis	ISOTOPIC RATIOS				CALCULATED AGES Ma			
	$^{208}Pb/^{232}Th$	± 1 sigma	$^{206}Pb/^{238}U$	± 1 sigma	$^{208}Pb/^{232}Th$	± 1 sigma	$^{206}Pb/^{238}U$	± 1 sigma
	Sample BZ345							
# 1	0.0049	0.0005	0.0158	0.0011	99	10	101	7
# 2	0.0049	0.0003	0.0156	0.0015	98	6	100	10
# 3	0.0042	0.0013	0.0144	0.0026	86	27	92	17
# 4	0.0049	0.0008	0.0152	0.0032	98	16	97	20
# 5	0.0047	0.0004	0.0153	0.0012	94	8	98	7
# 6	0.0039	0.0011	0.0157	0.0022	79	23	100	14
# 7	0.0046	0.0004	0.0163	0.0014	92	8	104	9
# 8	0.0047	0.0003	0.0156	0.0019	95	6	100	12
# 9	0.0045	0.0006	0.0150	0.0018	90	11	96	11
# 10	0.0047	0.0006	0.0148	0.0022	94	13	95	14

Discussion

The C–S fabrics at the contact between the Gemeric and Veporic Units have been previously interpreted as synkinematic and related to localization of deformation within the large scale detachment shear zone developed during unroofing and exhumation of the Veporic Dome (Hók et al. 1993; Plašienka 1993; Lupták et al. 2000; Janák et al. 2001). Indeed, the outcrop observations of C–S fabrics in the Veporic Unit show that lineations on both fabrics formed at a high angle to the fabrics intersection, implying its formation in a continuous kinematically related single-event. In the following discussion we bring the petrography-petrology, deformation microstructure and geochronology-based evidence suggesting that the studied S and C fabrics in the Veporic Unit were in contrast formed during two independent and kinematically unrelated tectonic events.

As already mentioned in the structural description, the studied S fabric is related to subhorizontal Alpine metamorphic foliation S_{A1} identified elsewhere throughout the Veporic Unit. In the basement, this fabric is associated with phengite, garnet, chloritoid, staurolite and kyanite-bearing assemblages with estimated PT conditions ranging between 5–11 kbar and 430–620 °C (e.g. Janák et al. 2001; Jeřábek et al. 2008). In addition, Jeřábek et al. (2008) documented that S_{A1} foliation is associated with the growth of Ca-rich garnets marked by prograde compositional zoning. The thermodynamic PT calculations revealed that the core to rim compositional changes in these garnets correspond to an increase in both pressure and temperature of up to 1.5 kbar and 50 °C (Jeřábek et al. 2008). On the basis of this evidence, they concluded that the formation of subhorizontal S_{A1} fabric is associated with burial of the Veporic Unit and not its exhumation as previously thought (Snopko 1967, 1971; Hók 1993; Plašienka 1993). Furthermore, it has been proposed that the Veporic Unit experienced an Early Cretaceous pure shear dominated E-W orogen-parallel flow in the lower crust triggered by the orogenic thickening due to overthrusting of the Gemeric Unit from the south (Jeřábek et al. 2008, 2012).

The thrusting along the Gemer-Vepor interface most likely led to the formation of imbricated structure revealed in the studied area by the bottom to top structural succession of basement orthogneiss, cover quartzite, garnet-bearing schist, chloritoid-kyanite schist and cover quartzite (Plašienka 1980, 1984). The subhorizontal S (S_{A1}) fabric in these rocks is associated with the growth of phengite and garnet-bearing assemblages (Figs. 5, 6). The garnets in the garnet-bearing schist sample BZ188 are characterized by two compositional varieties, which show identical chemical composition and zoning patterns as garnets that were previously reported from the Blh Valley to the southwest of the studied area (Vozárová & Krištín 1985; Korikovsky et al. 1990; Jeřábek et al. 2008). There, the garnet I cores and garnet II rims have been interpreted as Variscan and Alpine with PT estimates of ~580 °C at ~6 kbar and 510–540 °C at 8–9 kbar, respectively (Jeřábek et al. 2008). Based on the presence of the two generations of garnet in the studied schists, we interpret these rocks as parts of an imbricated Veporic basement that overthrusted Permian cover quartzites. This interpretation contrasts with the previously assumed Carboniferous deposition age and Veporic cover affinity (Planderová & Vozárová 1978; Vozárová & Vozár 1988) or Gemeric affinity of these schists (Plašienka 1984).

The observed transversal growth of chloritoid and kyanite with respect to the S fabric (Fig. 6d) documented in the chloritoid-kyanite schist suggests an inter-tectonic growth of this assemblage, thus distinctly separating the formation of S and C fabrics (see also Jeřábek et al. 2012). The chloritoid and kyanite-bearing assemblage in these schists has been used to constrain metamorphic PT conditions of 6–8 kbar and 530–560 °C (Lupták et al. 2000). The distinct white mica compositions revealed from the structurally lower and upper belt of cover quartzites (Figs. 1, 6) might indicate a difference in metamorphic grade that is most likely related to the hanging-wall and footwall position of the two belts with respect to the detachment shear zone cross-cutting the imbricated structure of the Gemeric-Veporic contact zone.

The C (S_{A2}) fabrics developed within this shear zone are defined by the lower grade chlorite- and muscovite-bearing assemblage (Figs. 5, 6) and show systematic top-to-the-east sense of shear observed either macroscopically (Fig. 2) or inferred from the inclination of quartz c-axis single girdle CPOs (Fig. 3b). These metamorphic and kinematic observations are consistent with the activity of the major detachment shear zone at the Gemer-Vepor boundary associated with exhumation and unroofing of the Veporic basement (Plašienka et al. 1999; Janák et al. 2001; Jeřábek et al. 2012). The Alpine

metamorphic field gradient across this detachment is characterized by rapid transition from low-grade metamorphism in the hanging-wall Gemeric Unit and Veporic Permo-Triassic Foederata cover to higher grade metamorphism within the footwall Permian quartzites and arkoses, and Veporic basement (Lupták et al. 2000, 2003). The main detachment is located within the Permian quartzitic-arkosic rocks as suggested by sharp metamorphic contrast between the muscovite-bearing arkose sample BZ172 and chloritoid-kyanite schist samples BZ183, BZ345 and BZ351 (for the position of the detachment see map in Fig. 1b). Towards the structural footwall in the west, the garnet-bearing basement schist (sample BZ188, Fig. 1) and underlying phengite-bearing Permian quartzite (sample BZ171, Fig. 1) are expected to record similar metamorphic conditions as the chloritoid-kyanite schists, which are in turn fairly similar to the basement metamorphic conditions in the west.

Quartz microstructures and textures from S and C fabrics corroborate well the above-discussed metamorphic character of both fabrics. Larger quartz grain size together with the transition from basal ⟨a⟩ to prism [c] slip systems within the S fabric point to medium metamorphic conditions and a water saturated environment (Okudaira et al. 1995), which is consistent with 550 °C obtained from the fabric opening thermometer (Kruhl 1996, 1998; Morgan & Law 2004). On the other hand, the smaller quartz grain size and the activity of rhomb ⟨a⟩ and prism ⟨a⟩ slip systems within the C fabric is characteristic for greenschist facies metamorphic conditions (e.g. Stipp et al. 2002). Following the interpretation of (Kilian et al. 2011), the inclination of the surface ODF maximum with respect to orientation of particle ODF maximum and C fabric (Fig. 3) is related to quartz crystal preferred orientation being dominated by rhomb ⟨a⟩ and prism ⟨a⟩ slip systems. Thus it is suggested that the surface ODF maximum together with overall monocline symmetry of surface ODF within the recrystallized C tails is promoted by a high amount of rhombohedral grain boundaries (Kuntcheva et al. 2006).

The dated monazite appears in close association with the inter-tectonic chloritoid and kyanite-bearing assemblage (Fig. 8a,b) indicating that monazite formation post-dates the burial-related S fabric. For this reason, the U-Th-Pb concordia age of 97 ± 4 Ma (Fig. 9) should be treated as the limiting age for the development of S fabric in this region. On the contrary, the C fabrics are associated with exhumation of the Veporic Unit and thus their formation age can be constrained by the previously published $^{40}Ar/^{39}Ar$ cooling ages. The in situ $^{40}Ar/^{39}Ar$ UV laser probe dating of white mica (Janák et al. 2001) from chloritoid-kyanite schist below the main detachment provided a mean age of 73 ± 8 Ma (± 1 sigma, sample HAN2). The same authors obtained similar ages of 72 ± 7 Ma and 77 ± 9 Ma from two other basement metapelite samples to the west of the studied area. On the other hand, a large number of $^{40}Ar/^{39}Ar$ cooling ages obtained by step-heating method from micas in the Veporic basement and cover concentrate between 87–83 Ma (Maluski et al. 1993; Dallmeyer et al. 1996; Kováčik et al. 1996; Putiš et al. 2009) indicating slightly older age of the exhumation process. One way or the other, these geochronological constraints indicate at least 10 million years time gap between the formation of the S and C fabrics.

Conclusions

Independent, kinematically unrelated C–S fabrics have been identified in the Alpine metamorphosed rocks of the Central Western Carpathians along the boundary between major basement-cover Gemeric and Veporic Units. The C–S fabrics occur within a major detachment shear zone, which cross-cuts the earlier imbricated structure related to overthrusting of the Gemeric Unit over Veporic. The evidence from deformation microstructures, petrology and geochronology, suggests that the S fabric formed during an Early Cretaceous subhorizontal lateral flow associated with overthrusting of the Gemeric Unit and burial of the Veporic Unit, while the C fabric originated via Late Cretaceous extensional shearing within the major detachment shear zone associated with exhumation of the Veporic Unit.

Acknowledgments: This work was financially supported by the research Grant from the Czech Science Foundation GACR 205/09/1041, the Ministry of Education, Youth and Sports of the Czech Republic Research Plan No. MSM0021620855, Charles University Science Foundation GAUK 5041/2012; and by Slovak Research and Development Agency (Project APVV-0080-11 to M. Janák), the Slovak Scientific Grant Agency VEGA (Project 2/0013/12 to M. Janák). F. Finger, R. Vojtko and D. Plašienka are thanked for their careful reviews.

References

Aftalion M., Bowes D.R., Dash B. & Dempster T.J. 1988: Late Proterozoic charnockites in Orissa, India: A U-Pb and Rb-Sr isotopic study. *J. Geol.* 96, 663–676.

Aftalion M., Bibikova E.V., Bowes D.R., Hopgood A.M. & Perchuk L.L. 1991: Timing of early Proterozoic collisional and extensional events in the granulite-gneiss-charnockite-granite complex, Lake Baikal, USSR: A U-Pb, Rb-Sr and Sm-Nd isotopic study. *J. Geol.* 99, 851–861.

Agard P., Augier R. & Monié P. 2011: Shear band formation and strain localization on a regional scale: Evidence from anisotropic rocks below a major detachment (Betic Cordilleras, Spain). *J. Struct. Geol.* 33, 114–131.

Berthé D., Choukroune P. & Jegouzo P. 1979: Orthogneiss, mylonite and noncoaxial deformation of granites: the example of the South Armorican Shear Zone. *J. Struct. Geol.* 1, 31–42.

Bibikova E.V., Cambel B., Korikovsky S.P., Broska I., Gracheva T.V., Makarov V.A. & Arakeljants M.M. 1988: U-Pb and K-Ar isotopic dating of Sinec (Rimavica) granites (Kohút zone of Veporides). *Geol. Zbor. Geol. Carpath.* 41, 427–436.

Dallmeyer R.D., Neubauer F., Handler R., Fritz H., Muller W., Pana D. & Putiš M. 1996: Tectonothermal evolution of the internal Alps and Carpathians: Evidence from $^{40}Ar/^{39}Ar$ mineral and whole-rock data. *Eclogae Geol. Helv.* 89, 203–228.

Faryad S.W. 1990: Gneiss-amphibolite complex of the Gemericum. *Miner. Slovaca* 22, 303–318.

Faryad S.W. 1991: Pre-Alpine metamorphic events in Gemericum. *Miner. Slovaca* 23, 395–402.

Faryad S.W. & Henjes-Kunst F. 1997: Petrological and K-Ar and ^{40}Ar–^{39}Ar age constraints for the tectonothermal evolution of the high-pressure Meliata unit, Western Carpathians (Slovakia). *Tectonophysics* 280, 141–156.

Gapais D. & White S.H. 1982: Ductile shear bands in naturally deformed quartzite. *Textures and Microstructures* 5, 1–17.

Heilbronner R. 2000: Automatic grain boundary detection and grain size analysis using polarization micrographs or orientation images. *J. Struct. Geol.* 22, 969–981.

Hovorka D., Ivan P., Jilemnická L. & Spišiak J. 1988: Petrology and geochemistry of metabasalts from Rakovec (Paleozoic of Gemeric Group, Inner Western Carpathians). *Geol. Zbor. Geol. Carpath.* 39, 395–425.

Hók J., Kováč P. & Madarás J. 1993: Extensional tectonics of the western part of the contact area between Veporicum and Gemericum (Western Carpathians). *Miner. Slovaca* 25, 172–176 (in Slovak with English summary).

Hraško Ľ., Kotov A.B., Salnikova E.B. & Kovach V.P. 1998: Enclaves in the Rochovce granite intrusion as indicators of the temperature and origin of the magma. *Geol. Carpathica* 49, 2, 125–138.

Janák M., Plašienka D., Frey M., Cosca M., Schmidt S.T., Lupták B. & Méres Š. 2001: Cretaceous evolution of a metamorphic core complex, the Veporic unit, Western Carpathians (Slovakia): P-T conditions and in situ $^{40}Ar/^{39}Ar$ UV laser probe dating of metapelites. *J. Metamorph. Geology* 19, 197–216.

Jeřábek P., Faryad S.W., Schulmann K., Lexa O. & Tajčmanová L. 2008: Alpine burial and heterogeneous exhumation of Variscan crust in the West Carpathians: insight from thermodynamic and argon diffusion modelling. *J. Geol. Soc. London* 165, 479–498.

Jeřábek P., Lexa O., Schulmann K. & Plašienka D. 2012: Inverse ductile thinning via lower crustal flow and fold-induced doming in the West Carpathian Eo-Alpine collisional wedge. *Tectonics*, doi:10.1029/2012TC003097.

Kamenický L. 1977: Contact metamorphism in the aureole of the Rimavica granite (West Carpathians Mts.). *Miner. Slovaca* 9, 3, 161–178.

Keller L.M. & Stipp M. 2011: The single-slip hypothesis revisited: Crystal-preferred orientations of sheared quartz aggregates with increasing strain in nature and numerical simulation. *J. Struct. Geol.* 33, 1491–1500.

Kilian R., Heilbronner R. & Stünitz H. 2011: Quartz microstructures and crystallographic preferred orientation: Which shear sense do they indicate? *J. Struct. Geol.* 33, 1446–1466.

Klinec A. 1966: On the structure and evolution of the Veporic crystalline unit. *Západ. Karpaty* 6, 7–28 (in Slovak).

Klinec A., Macek J., Dávidová Š. & Kamenický L. 1980: Rochovce Granite on contact between Gemerides and Veporides. *Geol. Práce, Spr.* 74, 130–112 (in Slovak with English summary).

Korikovsky S.P., Dupej J., Boronikhin V.A. & Zinovieva N.G. 1990: Zoned garnets and their equilibria in mica schists and gneisses of Kohút crystalline complex, Hnúšťa region, Western Carpathians. *Geol. Zbor. Geol. Carpath.* 41, 2, 99–124.

Košler J., Tubrett M. & Sylvester P. 2001: Application of laser ablation ICP-MS to U-Th-Pb dating of monazite. *Geostandards Newslett.* 25, 375–386.

Kováčik M., Kráľ J. & Maluski H. 1996: Metamorphic rocks in the Southern Veporicum basement: their Alpine metamorphism and thermochronologic evolution. *Miner. Slovaca* 28, 185–202 (in Slovak with English summary).

Kozur H. & Mock R. 1973: Zum Alter und zur tektonischen Stellung der Meliata-Serie des Slowakischen Karstes. *Geol. Zbor. Geol. Carpath.* 24, 365–374.

Kruhl J.H. 1996: Prism- and basal-plane parallel subgrain boundaries in quartz: a microstructural geothermobarometer. *J. Metamorph. Geology* 14, 581–589.

Kruhl J.H. 1998: Reply to: Okudaira T., Takeshita T. & Toriumi T. 1998: Prism- and basal-plane parallel subgrain boundaries in quartz: a microstructural geothermobarometer. *J. Metamorph. Geology* 16, 143–146.

Kuntcheva B., Kruhl J.H. & Kunze K. 2006: Crystallographic orientations of high-angle grain boundaries in dynamically recrystallized quartz: first results. *Tectonophysics* 421, 331–346.

Lexa O. 2003: Numerical approach in structural and microstructural analyses. *PhD Thesis*, *Charles University in Prague*, 1–138.

Lexa O., Schulmann K. & Ježek J. 2003: Cretaceous collision and indentation in the West Carpathians: View based on structural analysis and numerical modeling. *Tectonics* 22, 1066–1081.

Lister G.S. & Snoke A.W. 1984: S-C mylonites. *J. Struct. Geol.* 6, 617–638.

Lister G.S. & Williams P.F. 1979: Fabric development in shear zones: theoretical controls and observed phenomena. *J. Struct. Geol.* 1, 283–297.

Lupták B., Janák M., Plašienka D. & Schmidt S.T. 2000: Chloritoid-kyanite schists from the Veporic unit, Western Carpathians, Slovakia: implications for Alpine (Cretaceous) metamorphism. *Schweiz. Mineral. Petrogr. Mitt.*, 213–223.

Lupták B., Janák M., Plašienka D. & Schmidt S.T. 2003: Alpine low-grade metamorphism of the Permian-Triassic sedimentary rocks from the Vepor Superunit, western Carpathians: phyllosilicate composition and "crystallinity" data. *Geol. Carpathica* 54, 367–375.

Maluski H., Rajlich P. & Matte P. 1993: $^{40}Ar–^{39}Ar$ dating of the Inner Carpathians Variscan basement and Alpine mylonitic overprinting. *Tectonophysics* 223, 313–337.

Michalko J., Bezák V., Kráľ J., Huhma H., Mantari I., Vaasjoki M., Broska I. & Hraško L. 1998: U/Pb data of the Veporic granitoids (Western Carpathians). *Krystalinikum* 24, 91–104.

Montel J.-M., Foret S., Veschambre M., Nicollet C. & Provost A. 1996: Electron microprobe dating of monazite. *Chem. Geol.* 131, 37–53.

Morgan S.S. & Law R.D. 2004: Unusual transition in quartzite dislocation creep regimes and crystal slip systems in the aureole of the Eureka Valley-Joshua Flat-Beer Creek pluton, California: a case for anhydrous conditions created by decarbonation reactions. *Tectonophysics* 384, 209–231.

Okudaira T., Takeshita T., Hara I. & Ando J.-I. 1995: A new estimate of the conditions for transition from basal ⟨*a*⟩ to prism *[c]* slip in naturally deformed quartz. *Tectonophysics* 250, 31–46.

Panozzo R. 1983: Two-dimensional analysis of shape-fabric using projections of digitized lines in a plane. *Tectonophysics* 95, 279–294.

Panozzo R. 1984: Two-dimensional strain from the orientation of lines in a plane. *J. Struct. Geol.* 6, 215–221.

Panozzo Heilbronner R. & Pauli C. 1993: Integrated spatial and orientation analysis of quartz *c*-axes by computer-aided microscopy. *J. Struct. Geol.* 15, 369–382.

Passchier C.W. & Trouw R.A.J. 2005: Microtectonics. 2nd ed. *Springer Verlag*, 1–366.

Petrasová K., Faryad S.W., Jeřábek P. & Žáčková E. 2007: Origin and metamorphic evolution of magnesite-talc and adjacent rocks near Gemerská Poloma, Slovak Republic. *J. Geosci.* 52, 125–132.

Planderová E. & Vozárová A. 1978: Upper Carboniferous in southern Veporides. *Geol. Práce, Spr.* 70, 129–141.

Plašienka D. 1980: Nappe position of the Hladomorná dolina Group on the Foederata Group in the Dobšiná half-window. *Geol. Zbor. Geol. Carpath.* 31, 4, 609–617.

Plašienka D. 1984: Represents the Markuška nappe an interconnecting element between the Veporic and Gemeric units? *Miner. Slovaca* 16, 2, 187–193 (in Slovak with English summary).

Plašienka D. 1993: Structural pattern and partitioning of deformation in the Veporic Foederata cover unit (Central Western Carpathians). In: Rakús M. & Vozár J. (Eds.): Geodynamic model and deep structure of the Western Carpathians. *GÚDŠ,* Bratislava, 269–277.

Plašienka D., Grecula P., Putiš M., Kováč M. & Hovorka D. 1997: Evolution and structure of the Western Carpathians: an overview. In: Grecula P., Hovorka M. & Putiš M. (Eds.): Geological evolu-

tion of the Western Carpathians. *Miner. Slovaca — Monograph*, 1–24i.

Plašienka D., Janák M., Lupták B., Milovský R. & Frey R. 1999: Kinematics and metamorphism of a Cretaceous core complex: the Veporic unit of the Western Carpathians. *Phys. Chem. Earth (A)* 24, 651–658.

Platt J.P. 1979: Extensional crenulation cleavage. In: Cobbold P.R. & Fergusson C.C. (Eds.): Description and origin of spatial periodicity in tectonic structures. Report on a tectonic studies Group Conference. *J. Struct. Geol.* 1. Pergamon, Oxford–New York, International, 95–96.

Platt J.P. 1984: Secondary cleavages in ductile shear zones. *J. Struct. Geol.* 6, 439–442.

Platt J.P. & Vissers R.L.M. 1980: Extensional structures in anisotropic rocks. *J. Struct. Geol.* 2, 397–410.

Poller U., Uher P., Janák M., Plašienka D. & Kohút M. 2001: Late Cretaceous age of the Rochovce granite, Western Carpathians, constrained by U-Pb single zircon dating with cathodoluminiscence imaging. *Geol. Carpathica* 52, 41–47.

Ponce L.M.I. & Choukroune P. 1980: Shear zones in the Iberian Arc. *J. Struct. Geol.* 2, 63–68.

Putiš M., Frank W., Plašienka D., Siman P., Sulák M. & Biroň A. 2009: Progradation of the Alpidic Central Western Carpathians orogenic wedge related to two subductions: constrained by $^{40}Ar/^{39}Ar$ ages of white micas. *Geodinamica Acta* 1–3, 31–56.

Rozlosznik P. 1935: Die geologische Verhaeltnisse der Gegend von Dobšiná. *Geol. Hung.*, 1–118.

Schmid S.M. & Casey M. 1986: Complete fabric analysis of some commonly observed quartz c-axis patterns. In: Hobbs B.E. & Heard H.C. (Eds.): Mineral and rock deformation: Laboratory studies; the paterson volume, geophysical monograph series, vol. 36. *Amer. Geophys. Union*, Washington DC, 263–286.

Schönenberg R. 1946: Geologische Untersuchungen am Nordwestrand des Zips-Gömörer Erzgebirges (Karpaten). *Z. Dtsch. Geol. Gesell.* 98, 70–119.

Simpson C. & Schmid S.M. 1983: An evaluation criteria to deduce the sense of movement in sheared rocks. *Geol. Soc. Amer. Bull.* 94, 1281–1288.

Snopko L. 1967: Die Bedeutung der kleintektonischen Elemente bei der Lösung einiger geologischen Probleme des gemeriden Paläozoikum. *Sbor. Geol. Vied, Západ. Karpaty* 8, 7–49 (in Slovak with German summary).

Snopko L. 1971: The course of schistosity in the Paleozoic of the Spišsko-Gemerské Rudohorie Mountains. *Geol. Práce, Spr.* 57, 207–213 (in Slovak with English summary).

Stipp M. 2002: The eastern Tonale fault zone: a "natural laboratory" for crystal plastic deformation of quartz over a temperature range from 250 to 700 °C. *J. Struct. Geol.* 24, 1861–1884.

Sulák M., Kaindl R., Putiš M., Sitek J., Krenn K. & Tóth I. 2009: Chemical and spectroscopic characteristics of potassium white micas related to polystage evolution of the Central Western Carpathians orogenic wedge. *Lithos* 113, 709–730.

Tischendorf G., Rieder M., Foerster H.-J., Gottesmann B. & Guidotti C.V. 2004: A new graphical presentation and subdivision of potassium micas. *Mineral. Mag.* 68, 649–667.

Tomek Č. 1993: Deep crustal structure beneath the central and inner West Carpathians. *Tectonophysics* 226, 417–431.

Vozárová A. 1990: Development of metamorphism in the Veporic/Gemeric contact zone (Western Carpathians). *Geol. Zbor. Geol. Carpath.* 41, 475–502.

Vozárová A. & Krištín J. 1985: Changes in chemical composition of garnets and biotites from contact aureole of Alpine granitoides in southern part of Veporicum. *Západ. Karpaty, Sér. Mineral., Petrogr., Geochém., Metalogen.* 10, 199–221 (in Slovak with English summary).

Vozárová A. & Vozár J. 1988: Late Paleozoic in West Carpathians. *GÚDŠ*, Bratislava, 1–314.

Vrána S. 1964: Chloritoid and kyanite zone of Alpine metamorphism on the boundary of the Gemerides and the Veporides (Slovakia). *Krystalinikum* 2, 125–143.

Vrána S. 1966: Alpidische metamorphose der granitoiden und der Foederata Serie im mittelteil der Veporiden. *Zbor. Geol. Vied, Západ. Karpaty* 6, 29–84.

White S.H. 1979: Grain and sub-grain size variations across a mylonite zone. *Contr. Mineral. Petrology* 70, 193–202.

White S.H., Burrows S.E., Carreras J., Shaw N.D. & Humphreys F.J. 1980: On mylonites in ductile shear zones. *J. Struct. Geol.* 2, 175–187.